PROGRESS IN PHOTOVOLTAICS: RESEARCH AND APPLICATIONS
Prog. Photovolt: Res. Appl. 2007; **15**:727–740
Published online in Wiley InterScience (www.interscience.wiley.com) DOI: 10.1002/pip.796

Special Issue

Nanoscale Structure of Solar Cells Based on Pure Conjugated Polymer Blends

Sjoerd C. Veenstra[1,3]*,†, Joachim Loos[2,3] and Jan M. Kroon[1,3]
[1]*ECN Solar Energy, PO Box 1, 1755 ZG Petten, The Netherlands*
[2]*Laboratory of Materials and Interface Chemistry, and Laboratory of Polymer Technology, and Soft Matter CryoTEM Research Unit, Eindhoven University of Technology, PO Box 513, 5600 MB Eindhoven, The Netherlands*
[3]*Dutch Polymer Institute, PO Box 902, NL-5600 AX Eindhoven, The Netherlands*

This paper gives an overview of the status of photovoltaic devices based on blends of semiconducting polymers. The polymer blends form the bulk heterojunction in these photovoltaic devices. The fundamental mechanisms governing the performance of these devices are discussed as well as the specificities of these all-polymer solar cells. The morphology of the polymer blend layer is expected to influence the device performance of these bulk heterojunctions. An overview is presented of factors that influence the morphology of the active layer of polymer blend photovoltaic devices together with a summary of tools available to study the structure of this layer. An advanced electron microscopy technique is applied to study the morphology of polymer blends of MDMO-PPV and PCNEPV with differing molecular weights. It is shown that the molecular weight of the polymer influences the typical domain size from ∼200 nm down to less than 5 nm in these bulk heterojunction PV devices. No strong relation is observed between the typical length scale of the phase separated domains and the measured external quantum efficiency, indicating that the phases are intermixed. Copyright © 2007 John Wiley & Sons, Ltd.

KEY WORDS: organic photovoltaics; bulk heterojunction; morphology

Received 25 June 2007

INTRODUCTION

Since the discovery of the bulk heterojunction solar cell in 1995, photovoltaic (PV) devices based on conjugated polymers have attracted a lot of interest.[1–3] Polymer properties such as low weight and mechanical flexibility are expected to be advantageous for novel solar cell applications, especially for certain niche markets. In addition, polymer solutions exhibit in general good film forming properties which facilitates the use of high throughput production methods such as roll-to-roll processing to manufacture these cells on a large scale at low cost.

Over the last decade roughly three different device concepts were developed for polymer PV devices that meet the energetic, morphological and charge transport requirements.[3] The most intensively investigated concept is the system consisting of an electron donating polymer combined with an electron accepting fullerene. Devices made according to this concept currently reach 4–5% under standardized test conditions (AM1·5 G, 100 mW/cm^2).[4]

Another group of devices may be identified as 'hybrid devices'. In these devices, an inorganic semiconductor replaces the electron accepting fullerene. Examples of material combinations used for these

* Correspondence to: Sjoerd C. Veenstra, ECN Solar Energy, PO Box 1, 1755 ZG Petten, The Netherlands.
†E-mail: veenstra@ecn.nl

hybrid devices are P3HT:TiO_2,[5] MEH-PPV:TiO_2,[6] MDMO-PPV:ZnO[7,8] and P3HT:CdSe tetrapods.[9] Typical efficiencies obtained for these devices range from 0·4 to 1·6%, with the exception of devices prepared with CdSe tetrapods, yielding efficiencies of up to 2·8%.[9]

The third group of devices contains a blend of an electron donating and an accepting polymer. This concept may have an advantage over the other two types of polymer based PV devices, as in these devices both the donor and acceptor materials can contribute significantly to the overall light absorption. Ideally both components could cover complementary parts of the solar spectrum, which is hard to accomplish with the other types of polymer based PV devices. Efficiencies have been reported between 1·5 and 1·8% for devices based on this concept.[‡]

This paper concerns PV devices with a bulk heterojunction made of a phase separated polymer blend. A brief description of the status of the field is presented, followed by an overview of factors that influence the morphology of polymer blend PV devices together with a summary of tools available to study the polymer blend morphology. Finally, an advanced electron microscopy technique is applied to study the morphology of polymer blends of MDMO-PPV and PCNEPV with differing molecular weights. It is shown that the molecular weight of the polymers influences the typical domain size from ~200 nm down to less than 5 nm in these bulk heterojunction PV devices. No strong relation is observed between the typical length scale of the phase separated domains and the measured external quantum efficiency, indicating that the phases are intermixed.

CURRENT STATUS OF THE FIELD

The current status of the field will be briefly discussed by considering Equations 1 to 3:

$$\mathrm{EQE}(\lambda) = A(\lambda) \times \eta_{\mathrm{ED}} \times \eta_{\mathrm{CC}} \quad (1)$$

Equation 1 defines the external quantum efficiency (EQE(λ)) as the product of the absorbance of the blend film ($A(\lambda)$), the fraction of excitons which dissociates into free charges (η_{ED}) and the fraction of free charges collected at the electrodes. Note, experimentally, the EQE should be acquired with 1000 W/m^2 AM1·5 solar irradiance as bias light. The short-circuit current density (J_{sc}) is given by the overlap of the EQE spectrum and the tabulated AM1·5 spectrum ($S_{AM1·5}$)

$$J_{sc} = \mathrm{EQE}(\lambda) S_{AM1·5} d\lambda \quad (2)$$

The power conversion efficiency is:

$$\eta_{\mathrm{PCE}} = (J_{sc} V_{oc} \mathrm{FF}) / P_{AM1·5} \quad (3)$$

where V_{oc} and FF are the open circuit voltage and the fill factor, respectively, and $P_{AM1·5}$ the integrated power of the AM1·5 spectrum (1000 W/m^2). Note that the fill factor is defined as $\mathrm{FF} = (J_{MPP} V_{MPP})/(J_{sc} V_{oc})$ where J_{MPP} and V_{MPP} are the current density and voltage at the point in the fourth quadrant of the J–V curve where $|J \times V|$ reaches its maximum value.

Light absorption (A(λ))

Figure 1 shows the absorption spectrum of two representative polymers, applied in polymer PV devices.

The optical absorption coefficient (α) of conjugated polymers is typically around 1×10^7 m^{-1}·(Reference [10]). In order to absorb a large part of the available light in a polymer layer one thus typically requires an optical path of 100–200 nm. Since polymer PV devices consist of a reflective back contact, the thickness of these devices should be in the range of 50–100 nm.

The optical gap of the polymers used in Figure 1 is in the range of 2·1–2·3 eV. This gives a poor overlap with the solar spectrum: only 1 out of 6 photons in the AM1·5 spectrum carries enough energy to overcome

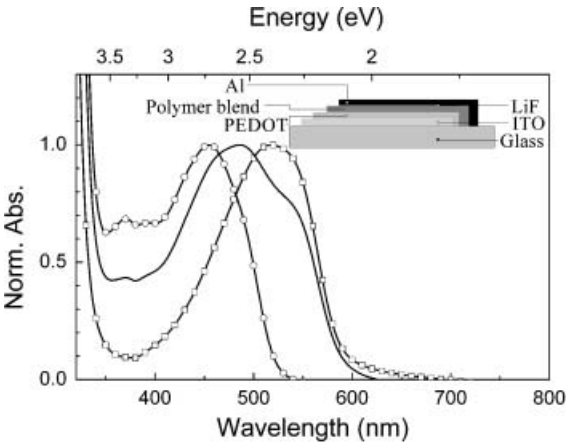

Figure 1. Normalised UV–Vis absorption, with respect to the absorption maximum in the visible part of the spectrum, of thin spin coated films on glass. MDMO-PPV (square), PCNEPV(circles) and a 1:1 blend, see Table I for chemical structures of these polymers. The inset gives a schematic presentation of a typical polymer blend PV device structure. Reprinted with permission from Reference 27. Copyright 2004 American Chemical Society

[‡]These devices will be discussed in more detailed below, for highest performances see References 11,25,28.

DOI: 10.1002/pip

the 2·1 eV band gap and contribute to the photocurrent in the PV device. It seems straightforward to improve polymer PV devices by applying polymers with a lower band gap. However these polymers are not widely available. McNeill *et al.* recently presented polymer PV devices consisting of two medium band gap polymers P3HT:F8TBT (see Table I for chemical structures of these polymers).[11] Both polymers have an optical gap of 1·9 eV. Despite a relatively low external quantum efficiency (EQE) of 26%, these devices gave short-circuit current densities of 4 mA/cm^2 and an overall performance of 1·8%, which is currently the highest reported power conversion efficiency for a polymer blend PV device.

Exciton dissociation (η_{ED})

The exciton binding energy (E_{eb}) of conjugated polymers exceeds the exciton binding energy of crystalline inorganic semiconductors by approximately an order of magnitude. In many inorganic semiconductors, the binding energy is comparable to, or lower than, the thermal energy at room temperature (kT~25 meV). In these materials, light absorption directly generates free charges under ambient conditions.[12] Organic and polymeric semiconductors, on the other hand, typically possess an exciton binding energy that is about 10 times kT.[13] As a consequence, organic solar cells need a mechanism to dissociate excitons into free charges.

A successful method to dissociate bound electron–hole pairs in organic semiconductors is the so-called donor/acceptor interface or bulk heterojunction.[1,2] This interface is formed between two organic semiconductors with dissimilar HOMO and LUMO levels. The donor material is the material with the lowest ionization potential, and the acceptor material the one with the largest electron affinity. If an exciton is created in the donor material and reaches the donor/acceptor interface, the electron will be transferred to the acceptor material and the hole will recede in the donor material provided that the system offers enough driving force for charge separation (in case the exciton was formed in the acceptor material, the hole is injected to the donor material and the electron remains in the acceptor) if the system provides enough driving force for charge separation.[§]

[§]This view might be oversimplified as the charge transfer mechanism may compete with a resonant energy transfer mechanism. However, if energy transfer precedes charge transfer in polymer PV blends, it will be followed by charge transfer, see for example Reference 14.

Donor/acceptor interfaces can be very efficient in separating excitons: in polymer:fullerene blends for example, the charge generation process takes place in the femtosecond time scale, while the reverse reaction, the charge recombination step, occurs in the microsecond range.[15] After exciton dissociation, a Coulomb interaction still exists between the charges located at either side of the donor–acceptor interface.[16] This interaction may assist (geminate) charge recombination. Independently from each other, Offermans *et al.* and Morteani *et al.* found evidence for the formation of exciplex states at polymer:polymer interfaces.[17,18] Their findings were recently confirmed by Yin *et al.*[19]

The importance of the exciplex decay channel strongly depends on the details of the state diagram and the rate constants of the transitions between these states. From these studies,[17–19] it is concluded that the generation of free charges is field and temperature dependent and competes with exciplex decay (via exciplex emission and/or population of the lowest T_1 state of the polymers).

Charge collection (η_{CC})

In general, the electron transport in polymer blend photovoltaic devices is not as well understood as the electron transport in PV devices based on polymer:-fullerene blends. Mandoc *et al.* reported recently on charge transport in MDMO-PPV:PCNEPV solar cells.[20] In this blend, the (zero-field) electron mobility of PCNEPV is 6×10^{-7} cm^2/Vs and strongly affected by the presence of electron trap sites. The hole mobility at room temperature of MDMO-PPV is similar to the value in a pure film: 5×10^{-6} cm^2/Vs. In contrast, in MDMO-PPV:PCBM blends (weight ratio 1:4) the hole mobility in MDMO-PPV is increased up to $1{\cdot}4 \times 10^{-4}$ cm^2/Vs and the electron mobility in PCBM is 2×10^{-3} cm^2/Vs.[21,22] Clearly, in MDMO-PPV: PCNEPV blends the electron and hole mobilities are significantly lower as compared to the values found in MDMO-PPV:PCBM blend. The low mobilities may affect the performance of the device. Yin *et al.* compared polymer bilayer and polymer blend devices (using M3EH-PPV or MEH-M3EH-PPV as donor and CN-ether-PPV as acceptor polymer).[19] They concluded that the photocurrent in polymer blend devices is mainly determined by charge carrier generation rather than by charge carrier recombination.

DOI: 10.1002/pip

Table I. Chemical structures of polymers used in polymer blend photovoltaic devices

Polymer	Chemical structure	Donor/Acceptor	Reference
Poly(para-phenylenevinylene)s			
MEH-PPV, MDMO-PPV, M3EH-PPV (depending on R, R')	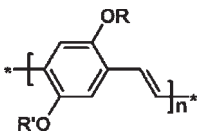	Donor	1, 2, 17, 19, 20, 25–28, 41, 49, 61
CN-PPV	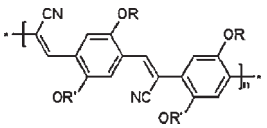	Acceptor	1, 2, 23
PCNEPV	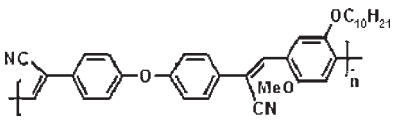	Acceptor	17, 18, 20, 25–27, 49, 61
Polythiophenes			
P3HT, POPT	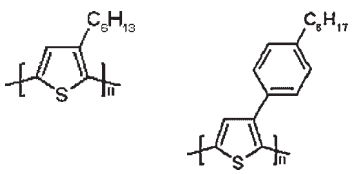	Donor, donor	11, 23, 24
Polyfluorene based copolymers			
TFB	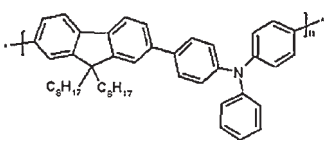	Donor	18, 30, 51
PFB	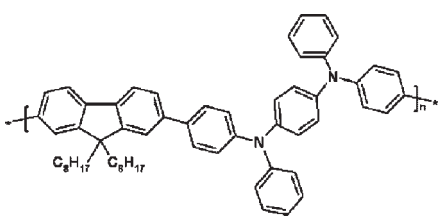	Donor	18, 32–34, 36, 50, 52
PF1CVTP	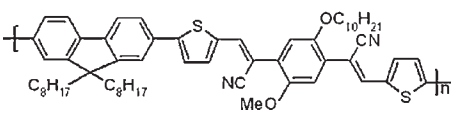	Acceptor	28
F8BT	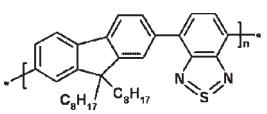	Acceptor	18, 24, 30, 32–34, 36, 50–52
F8TBT	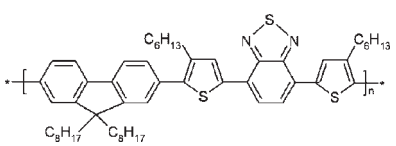	Acceptor	11

DOI: 10.1002/pip

One can speculate that the picture that may emerge from the above mentioned optical and transport measurements is one where the dissociation of the exciton mainly determines the quantum efficiency of the polymer blend PV device. The dissociation is field and temperature dependent as discussed above. The low mobility of the charge carriers facilitates geminate recombination as a weak Coulomb interaction remains between the electron–hole pair which stays in close proximity of the interface due to slow charge transport and/or charge trapping.

Power conversion efficiency (η_{PCE})

The strong influence of the electric field on the *J–V* curve is also reflected by the low fill factors observed in polymer blend PV devices: virtually all polymer blend PV devices show fill factors below 45% under one sun illumination intensity.[11,23–28] Currently, the best performing polymer blend PV devices yield maximum EQEs of up to 52%; AM1·5 (100 mW/cm^2) short-circuit currents between 3 and 4 mA/cm^2 and open-circuit voltages between 1 and 1·5 V. The highest reported AM1·5 (100 mW/cm^2) power conversion efficiencies range between 1·5 and 1·8%.[11,25,28] Besides the low fill factors, the performance is also limited by the sub-linear increase in the short-circuit current with illumination intensity, this is at least the case for PV devices based on MDMO-PPV and PF1CVTP. This is illustrated in Figure 2, which depicts the power conversion efficiency versus the illumination intensity measured on MDMO-PPV:PF1CVTP blend PV device. At one sun (AM1·5 100 mW/cm^2) a power conversion efficiency was measured of 1·8% for this cell.[‖] The power conversion efficiency increases with decreasing illumination intensity up to around 3% at an illumination intensity equal to 0·5–1 mW/cm^2. The increase in device performance is due to a combination of an increase in fill factor (from 0·39 to 0·48), with decreasing light intensity and the sub-linear increase in the short-circuit current density with increasing illumination intensity, as shown in the insets of Figure 2.

[‖]This was the best device, typical values for the η_{PCE} were between 1·5 and 1·7%. The photovoltaic parameters at AM1·5 (100 mW/cm^2) were: $V_{oc} = 1.39$ V, $J_{sc} = 3{\cdot}33$ mA/cm^2; FF = 0·39, $\eta_{PCE} = 1.8\%$.

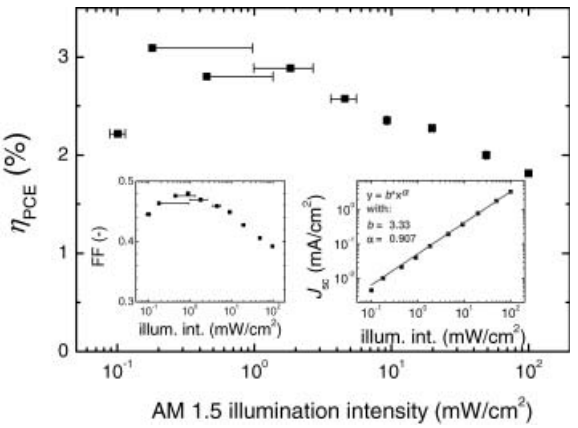

Figure 2. Power conversion efficiency (η_{PCE}) as function of the illumination intensity measured on a MDMO-PPV: PF1CVTP photovoltaic device (weight ratio 1:1, spin coated from chlorobenzene, layer thickness 40 ± 5 nm). The inset shows the fill factor (left) and short-circuit current density (right) as function of the AM1·5 illumination intensity

NANOSCALE STRUCTURE OF SOLAR CELLS BASED ON POLYMER BLENDS

Typical length scales in polymer bulk heterojunction solar cells

Some typical dimensions of polymer blend PV devices originate from general opto-electronic properties of conjugated polymers introduced in Section 'Current Status of the Field'. For efficient exciton dissociation, the photogenerated excitons should reach the donor/acceptor interface within their lifetime. Since the diffusion length of excitons in conjugated polymers is typically in the order of 5–10 nm, the phase separated blend should therefore possess a typical length scale of ~10 nm. For efficient charge collection, a continuous network of the donor and acceptor phases throughout the blend layer is required. A layered donor/acceptor structure would not yield efficient devices due to insufficient light absorption in the thin interfacial region (10–20 nm) where exciton dissociation is efficient. As discussed above, light absorption requires a polymer layer thickness of approximately 50 and 100 nm.

Thermodynamics of polymer solutions

The Flory–Huggins theory of mixing gives insight in the thermodynamic stability of polymer solutions.[29] The theory considers the change in Gibbs free energy

DOI: 10.1002/pip

(ΔG_m) of a system consisting of a polymer and a solvent.

$$\Delta G_m = \Delta H_m - T\Delta S_m \quad (4)$$

where ΔH_m and ΔS_m represent the change in enthalpy and entropy upon mixing, respectively. By using a lattice model in combination with several assumptions, it is possible to find an expression for the entropy of mixing for this polymer–solvent system.[¶] In the lattice model, each site is occupied either by a solvent molecule or by a polymer segment, where the volume of the polymer segment is similar to the volume of the solvent molecule. A restriction for the polymer segment is that it must be connected to two neighbouring polymer segments, occupying neighbouring lattice sites (except for the polymer end groups). The entropy of mixing can be expressed per 'segment' as:

$$\Delta S_m/nk = -[(\phi_1/N_1)\ln\phi_1 + (\phi_2/N_2)\ln\phi_2] \quad (5)$$

here k is Boltzmann's constant; ϕ_1 is the volume fraction of molecules of type 1, $\phi_1 = V_1/V$, where V_1 is the total volume occupied by molecules of type 1 and $V = V_1 + V_2$ is the total volume of the system. Similarly, ϕ_2 is the volume fraction of molecules of type 2. $n = N_1 n_1 + N_2 n_2$ is the total number of lattice points, or segments; n_1 and n_2 are the total number of molecules of type 1 and type 2, respectively. N_1 is the number of segments of which molecule 1 is supposed to consist of. For example, if molecules of type 1 are solvent molecules, N_1 is typically 1. If molecules of type 2 are polymers, N_2 is the number of segments used to describe these polymers in polymer segments with a similar volume (v) as the volume occupied by a solvent molecule 1. N_2 is proportional to the number of repeating units in the polymer and can be large, say 1000. From Equation 5 it becomes clear that the contribution of the polymer (molecules of type 2 in this example) to the change in entropy upon mixing is negligible if N_2 is large. This can be understood by realizing that after one of the segments of a polymer molecule is placed somewhere in volume V all the other segments of that particular molecule have the same freedom as in the original pure polymer state (although exceptions may occur).

[¶]We note here that the following expressions do not describe all the parameters influencing the thermodynamics of the thin polymer blend film. They are included here to indicate that the molecular weight strongly influences the entropy of the system.

The enthalpy of mixing can be expressed as[29]:

$$\Delta H_m = nkT\chi\phi_1\phi_2 \quad (6)$$

where χ is the Flory–Huggins parameter which may be loosely described as an interaction parameter between molecules of type 1 and 2. By combining Equations 4, 5 and 6 we obtain Equation 7 to describe the change in Gibbs free energy upon mixing polymer solutions:

$$\Delta G_m/nkT = (\phi_1/N_1)\ln\phi_1 + (\phi_2/N_2)\ln\phi_2 + \chi\phi_1\phi_2 \quad (7)$$

From Equation 7, it is clear that when both N_1 and N_2 become large, as is the case for polymer blends, the entropy term becomes very small. Since the enthalpy term is usually also small, this explains the observation that polymers do not mix in general, although numerous exceptions exist.

Toolbox to probe the morphology

A large number of experimental techniques have been used to investigate the morphology of the polymer blend layer in polymer blend PV devices. The listing presented below is not intended to be complete; it merely illustrates the available tools.

The use of *Optical Microscopic* techniques to study the morphology of the polymer blend may be divided into two classes: far- and near-field techniques. The far-field techniques have the disadvantage that they are diffraction limited, and therefore generally unable to resolve features smaller than 1 micron. However, these techniques are widely available and may give valuable information on the sample surface and bulk morphology.[24] Kim *et al.* used for example, fluorescence microscopy to study the composition of domains in a coarse phase separated blend.[30]

The diffraction limit can be overcome by applying near-field optical techniques. Stevenson and co-workers used fluorescence scanning near-field to characterize polymer blends for electroluminescent applications.[31] Their results show a rather low variation in the fluorescent intensity throughout the phase-separated blend attributed to a high extent of mixing within each phase. The obtained resolution was in the order of 300 nm. The data analysis was rather complicated since topological contrast influences the optical contrast. Arias *et al.* used a combination of far- and near-field optical techniques as well as atomic force microscopy (AFM) measurements. The authors identified in certain PFB:F8BT

DOI: 10.1002/pip

blends a hierarchy of micro- and nanometer-scale phase separated domains.[32] McNeill and co-workers reported on a related technique called near-field scanning photocurrent microscopy (NSPM), where the sample is locally illuminated using the fibre tip of a near-field scanning optical microscope (NSOM) and recording the locally induced photocurrent.[33]

Scanning probe microscopy (SPM) techniques are most applied to study the morphology of phase-separated blends in polymer blend PV devices.[23,27,34–36#] However, since the mechanical properties of the polymers in the blend are often very similar, contrast is frequently an issue. The typical lateral resolution that may be obtained is usually around 100 nm. Several SPM techniques have been derived from 'conventional' AFM. For example, conductive AFM (C-AFM) measures locally the electrical properties of the polymer blend,[41] where as Kelvin probe AFM measures locally the surface potential of the sample.[42–44] Since these scanning probe techniques exploit the electron donating or accepting properties of the photovoltaic blend, they obtain better contrast. The lateral resolution of these measurements techniques may be better than 100 nm.

Electron Microscopy (EM) has been applied successfully to study the morphology of polymer:fullerene blends.[45–48] However, applying this technique to polymer blends turned out less successful, again due to lack of contrast between the polymer phases.[49] An exception was presented by Blache *et al*., who applied environmental scanning EM (E-SEM) to PFB:F8BT blends and obtained well-resolved images.[50]

Advanced techniques determining the chemical composition of polymer blends on a nanometer scale are available. McNeill *et al.* recently utilized scanning transmission X-ray microscopy (STXM) to study both the topography and composition of TFB:F8BT samples with a lateral resolution better than 50 nm.[51,52] An alternative technique was recently applied by Loos and co-workers to blends of MDMO-PPV and PCNEPV. The technique is based on Energy Filtered Transmission EM (EF-TEM), where the chemical composition of the sample is measured by analyzing the electron energy loss spectrum of (inelastically scattered) electrons passing through the sample in the TEM experiment.[49] Results of these measurements are discussed below.

#These measurement techniques have also been applied to polymer:fullerene blends. See for example References 37–40 and 45–48.

Factors influencing the morphology of the photoactive layer polymer blend PV devices

Typically, the polymer blend layer in polymer composite PV devices is prepared by spin coating. The spin coat solution usually consists of an organic solvent (for example chloroform, toluene, chlorobenzene, xylene or ortho-di-chlorobenzene) with a low concentration of both polymers typically in the range between 0·2 and 2 weight per cent. During the spin coat process the *concentration* of the solution increases rapidly as the solvent evaporates, and since solvent evaporation is an endothermic process, the *temperature* of the solution decreases during the deposition step. Under these conditions the morphology of the deposited polymer blend layer depends both on the thermodynamic aspects, as well as on the kinetics of the film forming process.[53] Nevertheless, Equation 7 may still give clues about which process parameter may influence the blend morphology.

For example, the spin coat *solvent* influences the critical point, the point where the polymers start to phase separate. The solvent also influences the *evaporation rate* and thereby the concentration, the temperature of the solution during the film formation and the *layer thickness*. As an illustration, we plot in Figure 3, the measured short-circuit density against the vapour pressure of the solvent used to prepare PV devices with MDMO-PPV:PF1CVTP blends as active

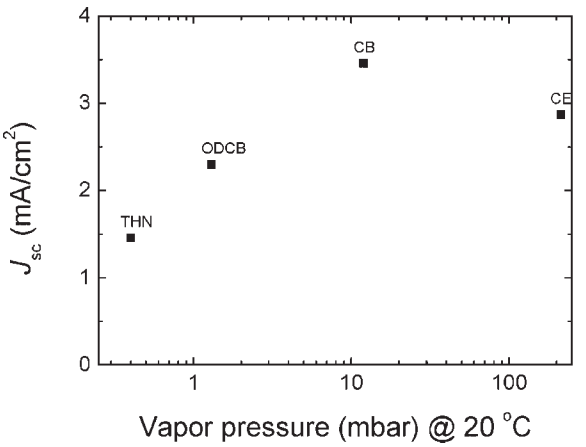

Figure 3. Short-circuit current density vs. the vapour pressure of the solvent used in the spin coat solution. The devices consist of a blend of MDMO-PPV:PF1CVTP (weight ration 1:1) spin coated from various solvents (THN: tetrahydronaphtalene; ODCB: ortho-dichloro-benzene; CB: chlorobenzene; CF: chloroform). All devices had a similar layer thicknesses of 32 ± 2 nm and were measured under a halogen lamp with an intensity of $1 \pm 0{\cdot}1$ sun

DOI: 10.1002/pip

layer. Clearly, the spin coat solvent influences the observed short-circuit current density of the PV device. This may not come as a surprise, however, explaining the observed differences is complicated and requires detailed knowledge of the optical, morphological and electronic properties of the devices.

Arias and co-workers investigated the morphology of PFB:F8BT blends spin coated from different solutions in great detail.[32] The authors observed that films processed from a chloroform solution yielded a finer phase separation (<100 nm) as films prepared from a xylene solution under otherwise similar conditions (phase separation on a scale >100 nm). They also observed that the EQE of the films prepared from the chloroform solution resulted in higher EQEs as compared to the samples prepared using a xylene solution. Yet, as the evaporation rate of the chloroform solution was decreased, by drop casting the chloroform solution in an environment with a high concentration of chloroform vapour, the phase separation occurred on a larger scale and samples prepared using this method yielded lower EQE values as the samples prepared by spin coating the chloroform solution. On the other hand, the EQE of samples prepared from a xylene solution could be improved by increasing the temperature of the sample/chuck combination prior to the spin coat step. The higher temperature of the sample increased the evaporation rate of xylene and resulted in a finer morphology. These measurements clearly indicate that solvent, evaporation rate and temperature influence the polymer blend morphology and may be applied to control the structure of the phase separated blend to a certain extend.

Another factor influencing the morphology of the polymer blend layer is the composition. However, this parameter also affects the optical and charge transport properties of the device. The overall effect of this parameter on the device performance is therefore rather complicated. Figure 4 depicts the short-circuit density against the volume fraction of the donor polymer in PV devices based on a blend of MDMO-PPV and PF1CVTP (all devices were prepared from chlorobenzene solutions and had similar layer thicknesses (45 ± 2 nm). *J–V* curves were measured under a halogen lamp with an intensity of $1 \pm 0{\cdot}1$ sun).

The relation between the composition of polymer:-fullerene PV devices, the morphology and performance has been investigated by several groups.[45–48,54] These studies have been important for developing and understanding the device physics of polymer:fullerene

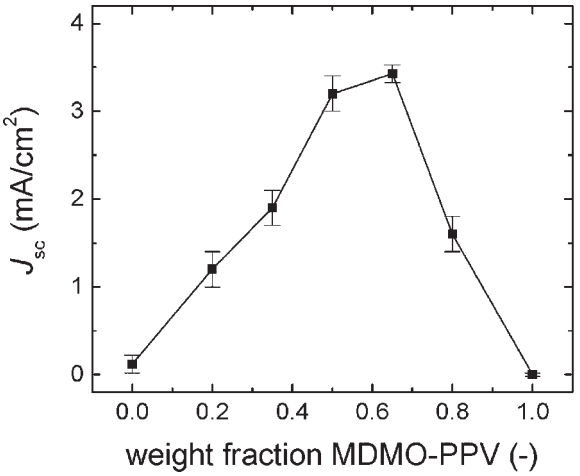

Figure 4. Short-circuit current density vs. composition of MDMO-PPV:PF1CVTP devices. These devices were spin coated from chlorobenzene and had similar layer thicknesses of 32 ± 2 nm. The PV devices were measured under a halogen lamp with an intensity of $1 \pm 0{\cdot}1$ sun

PV devices. Similar studies on polymer blend PV devices are unfortunately still scarce.[24]

Given that the polymer blend layer in polymer PV devices is only around 100 nm thick, the wetting behaviour at the polymer–substrate, and polymer–air interfaces plays an important role in the overall morphology as for example, shown for TFB:F8BT blends by Kim and co-workers.[30] It is possible to alter the interaction at the substrate–polymer blend interface by application of a self assembled monolayer (SAM) on top of the substrate. Furthermore, these SAMs can be printed with high lateral resolution, it should be possible to induce phase separation in a blend by applying a nanoscale, patterned SAM on the substrate.[53]

By careful control over the factors influencing the morphology of polymer blends during film formation, it is possible to optimize phase separation in polymer blend films for certain applications. Perhaps, a more elegant approach towards morphological control on the nanometer scale is the application of block copolymers. *Block copolymers* have a 'built-in' tendency to phase separate on a scale which is related to the length of the blocks of the polymer.[55] Attempts to exploit donor–acceptor block copolymers for photovoltaic applications have been limited, both in number and success.[56–60]

Another way to make the blend morphology less sensitive to the film forming conditions was introduced by Kietzke and co-workers.[61] The method involves

DOI: 10.1002/pip

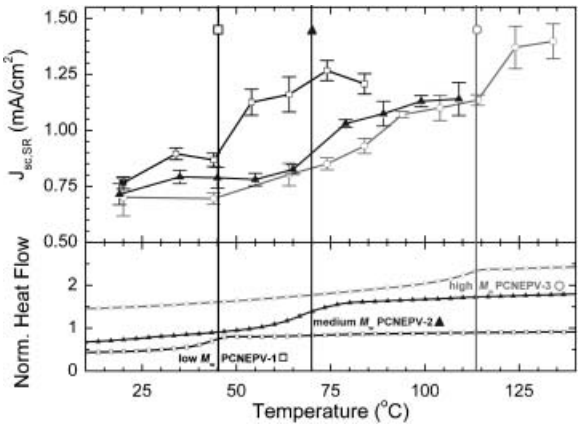

Figure 5. The top panel shows the calculated AM 1·5 current density at 1 sun ($J_{sc,SR}$), as calculated from the spectral response of the sample (see equation 2), as a function of the sample anneal temperature for three types of polymer blends differing in the molecular weight (M_w) of the PCNEPV polymer: black, open squares represent the values obtained with a blend containing the low M_w PCNEPV (PCNEPV-1), dark gray, closed triangles represent the medium M_w PCNEPV (PCNEPV-2), and gray, open circles represent the high M_w PCNEPV (PCNEPV-3). Note, the spectral responses of the samples were recorded after the samples reached room temperature. The lower panel shows the differential scanning calorimetry (DSC) scan of the three PCNEPV batches. The vertical lines are a guide for the eye. See Table II for additional information on the polymer bacthes. Reprinted with permission from Reference 26. Copyright 2004 American Chemical Society

polymer nanoparticles prepared in a micro-emulsion. The nanoparticles contain either the pure donor polymer, the acceptor polymer or a blend. The size of the nanoparticles forms an upper limit of the phase-separated domains in the polymer blend PV devices. Devices prepared from these polymer nanoparticles showed reasonable efficiencies.

Even after the polymer blend layer is formed, it is often still possible to alter the morphology. As mentioned above, it is likely that the as-prepared film is not at thermodynamic equilibrium. Generally, the morphology of a polymer blend film is 'frozen' below the glass transition temperature (T_g). In order to accommodate morphological changes within a reasonable timescale, the temperature of the sample should be above T_g of at least one of the polymers in the composite, often people refer to this as '*annealing*'. Once the temperature of the film is above T_g, the polymer chains become more mobile and may be able to redistribute to decrease the Gibbs free energy of the system. The redistribution of polymer chains is accompanied with a morphological change. The effect of this process may influence the PV characteristics of the devices as illustrated by Figure 5.[27,62]

The lowest trace depicted in the top panel of Figure 5 was recorded on a MDMO-PPV:PCNEPV device with the low molecular weight PCNEPV derivative. The transition in the DSC scan is found around 45°C; close to the transition observed in the short-circuit current density of the blend based on the same PCNEPV. For the medium molecular weight PCNEPV both transitions (T_g and $J_{sc,SR}$) coincide around 70°C. The DSC trace of the high molecular weight PCNEPV (top trace in lower panel of Figure 5) gives a transition around 115°C, corresponding to the high-temperature transition in the current density plot. The gradual increase in short-circuit current density found around 80°C is related to the T_g of MDMO–PPV as determined by thermal dynamic mechanical analysis (DMTA) on the MDMO–PPV used in these experiments. Temperature dependent AFM measurements on these blends indeed reveal a morphology change when the sample is annealed above the T_g.

Figure 5 also shows that T_g depends on the molecular weight of the polymer. As discussed in Sub-section 'Thermodynamics of polymer solutions', the *molecular weight* of the polymer influences the entropy of the system. Since both the temperature, and thus T_g, as well as the entropy of mixing are parameters that (may) influence the morphology of spin coated polymer blend films, it is anticipated that the molecular weight of the polymer may also affect the domain size. This will be discussed in the next section.

EFFECT OF MOLECULAR WEIGHT ON MORPHOLOGY OF POLYMER BLEND AND PHOTOVOLTAIC PERFORMANCE

Table II gives a summary of some of the polymer properties of three batches of acceptor polymer used to investigate the influence of the molecular weight on the morphology and PV properties of polymer donor–acceptor blends. Table I gives the molecular structure of both polymers. The PCNEPV derivatives have two nitrogen atoms in each repeat unit of their backbones. The donor polymer does not contain nitrogen atoms. This difference in chemical composition is exploited

DOI: 10.1002/pip

Table II. Specification of the acceptor polymer properties molecular weight M_w, polydispersity index (PDI), glass transition temperature T_g, and the resulting domain sizes when blended with the donor polymer MDMO-PPV 1:1 by weight as observed with EF-TEM measurements

Sample	Acceptor PCNEPV	M_w (g/mol)	PDI	T_g (°C)	Domain size (nm)
1	PCNEPV -1	3,500	1·7	45	<5
2	PCNEPV -2	48,000	4	70	20–50
3	PCNEPV -3	113,500	2·8	115	∼200

EF-TEM. In EF-TEM, the electron energy loss of the inelastically scattered electrons is analyzed. The electron energy loss spectrum (EELS) contains characteristic features of atomic core levels. This enables quantitative two-dimensional elemental distribution mapping with nanometer resolution and high chemical accuracy.

Figure 6 gives representative EF-TEM images of the polymer blends in which the molecular weight of the PCNEPV polymer are varied. For medium molecular weight small and homogenously distributed PCNEPV domains having sizes of about 20–50 nm are observed in the MDMO-PPV matrix (Figure 6b). For low molecular weight MDMO-PCNEPV (Table II, entry 1) a homogeneous film without distinct phase separation can be observed (Figure 6a). In contrast, high molecular weight MDMO-PCNEPV (Table II, entry 3, Figure 6c) results in a large-scale phase separation with relatively large PCNEPV domains (domain diameter ∼200 nm).

Looking at Figure 6b, it is clear that the PCNEPV domains do not fill 50% of sample 2, as one might expect in a 1:1 MDMO-PPV/PCNEPV blend. This is a clear indication for intermixing between the phases. The term nitrogen-rich phase has to be interpreted in such a way that only enrichment of nitrogen can be detected, which includes that PCNEPV molecules can still be present in the less-rich nitrogen regions of the sample. This is corroborated by the fact that all these blends show complete fluorescence quenching.

Figure 7 presents the EQE spectra of the three samples. The differences between the spectra with decreasing molecular weight of the MDMO-PCNEPV are subtle: a small increase in the maximum value of the EQE is observed, accompanied with a shift of spectral weight to longer wavelengths. The differences in the EQEs, are reflected in the calculated current:

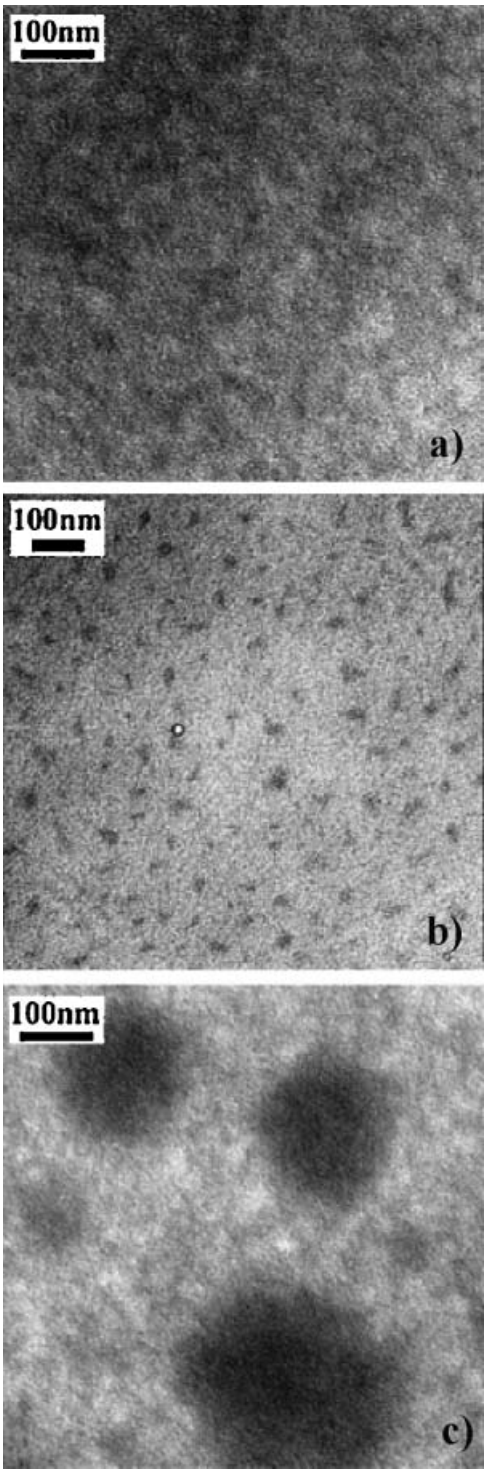

Figure 6. Zero-loss filtered TEM images of thin MDMO-PPV/PCNEPV blend film samples: (a) sample 1 with low M_w PCNEPV derivative, (b) sample 2 with medium M_w PCNEPV derivative and (c) sample 3 with high M_w PCNEPV derivative

DOI: 10.1002/pip

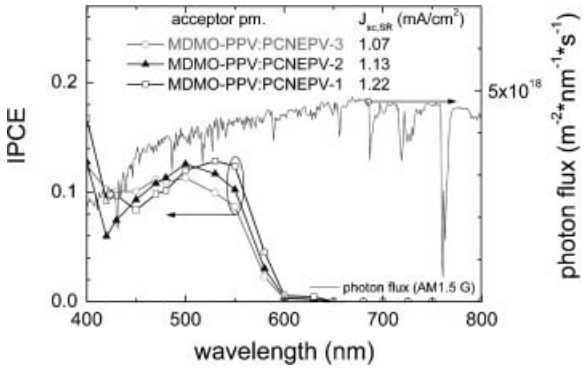

Figure 7. EQE spectra of all-polymer blend based photovoltaic devices differing in the molecular weight of the acceptor polymer (see Table II) and the tabulated AM1·5 spectrum (100 mW/cm^2). The black line with the open squares represents the EQE values obtained on a device with a blend containing the low M_w PCNEPV (PCNEPV-1), dark gray, closed triangles represent the data recorded on a device with the medium M_w PCNEPV (PCNEPV-2), and gray, open circles the EQE obtained with a device prepared with the high M_w PCNEPV (PCNEPV-3) $J_{sc,SR}$ is the calculated short-circuit current determined using equation 2

with decreasing molecular weight of the acceptor polymer, the calculated current increases (Table III). Note that both the shape of the spectrum and the magnitude of the EQE spectrum contribute to an increase in the calculated current, see Figure 7.

One could speculate that phase separation with homogenously distributed small PCNEPV domains, (as found in sample 2), or no detectable domains at all (sample 1), is expected to be favourable for efficient exciton dissociation. The morphology as obtained in sample 2 seems most suitable for both efficient exciton dissociation and charge collection, as charge collection in sample 1 may suffer from recombination given that the electron and hole transport channels are not well separated. The phase separation observed in sample 3 would be on a length scale, too large for efficient exciton dissociation.

However, the PV measurements (Table III) only show small differences in EQE data and corresponding short-circuit densities. Relating the obtained morphological data of photoactive layers with the short-circuit current densities; it is concluded that the large differences in morphology of the investigated photoactive layers did not result in large differences in the short-circuit current densities. This conclusion is in agreement with the fact that the fluorescence of these samples is quenched and the quantitative analysis of the EF-TEM data, indicating that intermixing plays an important role in these polymer blends. We note that McNeill and co-workers studied polyfluorene based polymer blends with similar resolution. They also observed significant intermixing down to the nanoscale in the polymer composite.[51,52]

CONCLUSIONS

A brief overview of the field of all-polymer blend PV devices is presented. These devices are based on the concept of a bulk heterojunction. The length scale of the phase separated domains is therefore expected to be of importance for the device performance. A number of factors are discussed which influence the morphology in the blend and may give some control of the domain sizes in the bulk heterojunction.

The morphology of a blend consisting of MDMO-PPV and PCNEPV is investigated using EF-TEM. It is shown that EF-TEM is able to monitor size and distribution of the PCNEPV phase in these functional polymer blends. Based on the morphology results obtained, we have demonstrated that adjusting the organization of functional blends by variation of the molecular weight of their components is possible. However, we did not observe a strong relation between the sizes of the phase separated domains and the observed short-circuit currents. This weak dependence is attributed to the intermixing of the two polymer phases, which is in agreement with fluorescent data.

Table III. Overview of the photovoltaic parameters measured on MDMO-PPV:PCNEPV based PV devices measured under approximately one sun illumination intensity

Sample	Acceptor Polymer	M_w (g/mol)	EQE (%)	V_{oc} (V)	$J_{sc,SR}$ (mA/cm^2)	FF	MPP (mW/cm^2)
OSC 1	PCNEPV-1	3,500	12·8	1·30	1·22	0·32	0·50
OSC 2	PCNEPV-2	48 000	12·6	1·25	1·13	0·30	0·42
OSC 3	PCNEPV-3	113 500	11·3	1·35	1·07	0·27	0·38

The devices differ in the molecular weight of the acceptor polymer. $J_{sc,SR}$ is the calculated short-circuit current determined using Equation 2. MPP abbreviates maximum power point.

DOI: 10.1002/pip

EXPERIMENTAL

Detailed information on the different batches and derivatives can be found elsewhere.[27] The molecular weight distributions were determined by gel permeation chromatography (GPC) using polystyrene as standard. The glass transition temperatures were determined by differential scanning calorimetry (DSC) measurements using a heating rate of 20°C/min. Similar to working devices, samples for energy-filtered transmission electron microscopy (EF-TEM) investigations were prepared on glass substrates with patterned indium tin oxide (ITO) electrodes see Reference [27]. The concentration and spin coating conditions were adjusted to form an active layer with thickness between 30 nm and 40 nm. PV and EF-TEM samples were annealed before the measurements.

For EF-TEM investigations the active blend layer was removed from the substrate by selective floating on water, and subsequently deposited on a 400-mesh copper grid. EF-TEM measurements were conducted on a Philips CM20 TEM equipped with a Gatan Image Filter (GIF 200) applying a 3 mm aperture for imaging and an energy resolution of better than 1 eV in spectroscopy mode. The photovoltaic devices were characterized as discussed in Reference [27].

Acknowledgements

The authors like to thank Xiaoniu Yang (State Key Laboratory of Polymer Physics and Chemistry, Changchun Institute of Applied Chemistry, Chinese Academy of Sciences, Changchun, P. R. China). A special thanks from one of the authors (J. L.) is extended to the whole team of FELMI (Forschungszentrum für Elektronenmikroskopie, Graz, Austria) for their indefatigable readiness for discussions and technical as well as personal support.

REFERENCES

1. Yu G, Heeger AJ. Charge separation and photovoltaic conversion in polymer composites with internal donor-acceptor heterojunctions. *Journal of Applied Physics* 1995; **78**: 4510–4515.
2. Halls JJM, Walsh CA, Greenham NC, Marseglia E, Friend RH, Moratti SC, Holmes AB. Photoinduced absorption and excitation spectra studies of excited states in a cyano-derivative of poly(p-phenylenevinylene). *Nature* 1995; **376**: 498–500.
3. MRS Bull. *Special issue on organic based photovoltaics*, edited by SE Shaheen, DS Ginley, GE Jabbour. (2005); **30**: 10–52
4. Green MA, Emery K, Hisikawa Y, Warta W. Solar cell efficiency tables (version 30). *Progress in Photovoltaics: Research and Applications* 2007; **15**: 425–430.
5. Coakley KM, Liu Y, McGehee MD, Frindell KM, Stucky GD. Photovoltaic cells made from conjugated polymers infiltrated into mesoporous titania. *Advanced Functional Materials* 2003; **13**: 301–306.
6. Zheng Z, Yang M, Liu Y, Zhang B. A large interconnecting network within hybrid MEH-PPV/TiO2 nanorod photovoltaic devices. *Nanotechnology* 2006; **17**: 5387–5392.
7. Beek WJE, Wienk MM, Janssen RAJ. Hybrid solar cells from regioregular polythiophene and ZnO nanoparticles. *Advanced Materials* 2004; **16**: 1009–1013.
8. Koster LJA, van Strien WJ, Beek WJE, Blom PWM. Device operation of conjugated polymer/zinc oxide bulk heterojunction solar cells. *Advanced Functional Materials* 2007; **17**: 1297–1302.
9. Sun B, Snaith HJ, Dhoot AS, Westenhoff S, Greenham NC. Vertically segregated hybrid blends for photovoltaic devices with improved efficiency. *Journal of Applied Physics* 2005; **97**: 014914/1-6.
10. Quist PAC, Savenije TJ, Koetse MM, Veenstra SC, Kroon JM, Siebbeles LDA. The effect of annealing on the charge-carrier dynamics in a polymer/polymer bulk heterojunction for photovoltaic applications. *Advanced Functional Materials* 2005; **15**: 469–474.
11. McNeill CR, Abrusci A, Zaumseil J, Wilson R, McKiernan MJ, Burroughes JH, Halls JJM, Greenham NC, Friend RH. Dual electron donor/electron acceptor character of a conjugated polymer in efficient photovoltaic diodes. *Applied Physics Letters* 2007; **90**: 193506/1-6.
12. Bube RH. *Photoelectronic Properties of Semiconductors*. Cambridge University Press: Cambridge, 1992.
13. Pope M, Swenberg CE. *Electronic Processes in Organic Crystals and Polymers*. Oxford University Press: Oxford, 1999.
14. Liu Y-X, Summers MA, Scully SR, McGehee MD. Resonance energy transfer from organic chromophores to fullerene molecules. *Journal of Applied Physics* 2006; **99**: 093521/1-4.
15. Smilowitz L, Sariciftci NS, Wu R, Gettinger C, Heeger AJ, Wudl F. Photoexcitation spectroscopy of conducting polymer-C60 fullerene composites: photoinduced electron transfer. *Physical Review B* 1993; **47**: 13835–13842.
16. Mihailetchi VD, Koster LJA, Hummelen JC, Blom PWM. Photocurrent generation in polymer-fullerene bulk heterojunctions. *Physical Review Letters* 2004; **93**: 216601/1-4.
17. Offermans T, van Hal PA, Meskers SCJ, Koetse MM, Janssen RAJ. Exciplex dynamics in a blend of p-conjugated polymers with electron donating and

DOI: 10.1002/pip

accepting properties: MDMO-PPV and PCNEPV. *Physical Review B* 2005; **72**: 045213/1-13.
18. Morteani AC, Sreearunothai P, Herz LM, Friend RH, Silva C. Exciton regeneration at polymeric semiconductor heterojunctions. *Physical Review Letters* 2004; **92**: 247402/1-4.
19. Yin C, Kietzke T, Neher D, Hörhold H-H. Photovoltaic properties and exciplex emission of polyphenylenevinylene-based blend solar cells. *Applied Physics Letters* 2007; **90**: 092117/1-3.
20. Mandoc MM, Veurman W, Koster LJA, Koetse MM, Sweelssen J, de Boer B, Blom PWM. Charge transport in MDMO-PPV:PCNEPV all-polymer solar cells. *Journal of Applied Physics* 2007; **101**: 104512/1-5.
21. Melzer C, Koop EJ, Mihailetchi VD, Blom PWM. Hole transport in poly(phenylenevinylene)/methanofullerene bulk-heterojunction solar cells. *Advanced Functional Materials* 2004; **14**: 865–870.
22. Mihailetchi VD, van Duren JKJ, Blom PWM, Hummelen JC, Janssen RAJ, Kroon JM, Rispens MT, Verhees WJH, Wienk MM. Electron transport in a methanofullerene. *Advanced Functional Materials* 2003; **13**: 43–46.
23. Granström M, Petritsch K, Arias AC, Lux A, Andersson MR, Friend RH. Laminated fabrication of polymeric photovoltaic diodes. *Nature* 1998; **395**: 257–260.
24. Kim Y, Cook S, Choulis SA, Nelson J, Durrant JR, Bradley DDC. Organic photovoltaic devices based on blends of regioregular poly(3-hexylthiophene) and poly(9,9-dioctylfluorene-co-benzothiadiazole). *Chemistry of Materials* 2004; **16**: 4812–4818.
25. Kietzke T, Hörhold H-H, Neher D. Efficient polymer solar cells based on M3EH-PPV. *Chemistry of Materials* 2005; **17**: 6532–6537.
26. Chasteen SV, Härter JO, Rumbles G, Scott JC, Nakazawa Y, Jones M, Hörhold H-H, Tillman H, Carter SA. Comparison of blended versus layered structures for poly(p-phenylene vinylene)-based polymer photovoltaics. *Journal of Applied Physics* 2006; **99**: 033709/1-10.
27. Veenstra SC, Verhees WJH, Kroon JM, Koetse MM, Sweelssen J, Bastiaansen JJAM, Schoo HFM, Yang X, Alexeev A, Loos J, Schubert US, Wienk MM. Photovoltaic properties of a conjugated polymer blend of MDMO-PPV and PCNEPV. *Chemistry of Materials* 2004; **16**: 2503–2508.
28. Koetse MM, Sweelssen J, Hoekerd KT, Schoo HFM, Veenstra SC, Kroon JM, Yang X, Loos J. Efficient polymer: polymer bulk heterojunction solar cells. *Applied Physics Letters* 2006; **88**: 083504/1-3.
29. Challa G. *Polymer chemistry, an introduction*. Ellis Horwood Limited: Hemel Hempstead, UK, 1999; Flory PJ, *Journal of Chemical Physics* 1941; **9**: 660.
30. Kim J-S, Ho PK, Murphy CE, Friend RH. Phase separation in polyfluorene-based conjugated polymer blends: lateral and vertical analysis of blend spin-cast thin films. *Macromolecules* 2004; **37**: 2861–2871.
31. Stevenson R, Riehn R, Milner RG, Richards D, Moons E, Kang D-J, Blamire M, Morgado J, Cacialli F. *Applied Physics Letters* 2001; **79**: 833.
32. Arias AC, MacKenzie JD, Stevenson R, Halls JJM, Inbasekaran M, Woo EP, Richards D, Friend RH. Photovoltaic performance and morphology of polyfluorene blends: a combined microscopic and photovoltaic investigation. *Macromolecules* 2001; **34**: 6005–6013.
33. McNeill CR, Frohne H, Holdsworth JL, Dastoor PC. Near-field scanning photocurrent measurements of polyfluorene blend devices: directly correlating morphology with current generation. *Nano Letters* 2004; **4**: 2503.
34. Snaith HJ, Arias AC, Morteani AC, Silva C, Friend RH. Charge generation kinetics and transport mechanisms in blended polyfluorene photovoltaic devices. *Nano Letters* 2002; **2**: 1353–1357.
35. Corcoran N, Arias AC, Kim JS, MacKenzie JD, Friend RH. Increased efficiency in vertically segregated thin-film conjugated polymer blends for light-emitting diodes. *Applied Physics Letters* 2003; **82**: 299–301.
36. Arias AC, Corcoran N, Banach M, Friend RH, MacKenzie JD, Huck WTS. Vertically segregated polymer-blend photovoltaic thin-film structures through surface-mediated solution processing. *Applied Physics Letters* 2002; **80**: 1695–1697.
37. Douhéret O, Lutsen L, Swinnen A, Breselge M, Vandewal K, Goris L, Manca J. Nanoscale electrical characterization of organic photovoltaic blends by conductive atomic force microscopy. *Applied Physics Letters* 2006; **89**: 032107/1-3.
38. Hoppe H, Glatzel T, Niggemann M, Hinsch A, Lux-Steiner M Ch, Sariciftci NS. Kelvin probe force microscopy study on conjugated polymer/fullerene bulk heterojunction organic solar cells. *Nano Letter* 2005; **5**: 269–274.
39. Coffey DC, Ginger DS. Time-resolved electrostatic force microscopy of polymer solar cells. *Nature Materials* 2006; **5**: 735–740.
40. van Duren JKJ, Yang X, Loos J, Bulle-Lieuwma CWT, Sieval AB, Hummelen JC, Janssen RAJ. Relating the morphology of poly(p-phenylene vinylene)/methanofullerene blends to solar cell performance. *Advanced Functional Materials* 2004; **14**: 425–434.
41. Alexeev A, Loos J, Koetse MM. Nanoscale electrical characterization of semiconducting polymer blends by conductive atomic force microscopy (C-AFM). *Ultramicroscopy* 2006; **106**: 191–199.
42. Chiesa M, Burgi L, Kim J-S, Shikler R, Friend RH. Correlation between surface photovoltage and blend morphology in polyfluorene-based photodiodes. *Nano Letters* 2005; **5**: 559–563.

DOI: 10.1002/pip

43. Palermo V, Ridolfi G, Talarico AM, Favaretto L, Barbarella G, Camaioni N, Samori P. A kelvin probe force microscopy study of the photogeneration of surface charges in all-thiophene photovoltaic blends. *Advanced Functional Materials* 2007; **17**: 472–478.
44. Palermo V, Liscio A, Gentilini D, Nolde F, Mullen K, Samori P. Scanning probe microscopy investigation of self-organized perylenetetracarboxdiimide nanostructures at surfaces: structural and electronic properties. *Small* 2007; **3**: 161–167.
45. Hoppe H, Sariciftci NS. Morphology of polymer/fullerene bulk heterojunction solar cells. *Journal of Materials Chemistry* 2006; **16**: 41–61.
46. van Duren JKJ, Loos J, Morrissey F, Leewis CM, Kivits KPH, van IJzendoorn LJ, Rispens MT, Hummelen JC, Janssen RAJ. In-situ compositional and structural analysis of plastic solar cells. *Advanced Functional Materials* 2002; **12**: 665–669.
47. Bertho S, Haeldermans I, Swinnen A, Moons W, Martens T, Lutsen L, Vanderzande D, Manca J, Senes A, Bonfiglio A. Influence of thermal ageing on the stability of polymer bulk heterojunction solar cells. *Solar Energy Materials and Solar Cells* 2007; **91**: 385–389.
48. Martens T, D'Haen J, Munters T, Goris L, Beelen Z, Manca J, D'Olieslaeger M, Vanderzande D, Schepper LD, Andriessen R. Isclosure of the nanostructure of MDMO-PPV:PCBM bulk hetero-junction organic solar cells by a combination of SPM and TEM. *Proceedings of the MRS Spring Meeting*, San Francisco, 2002; **725**: 169–175.
49. Loos J, Yang X, Koetse MM, Sweelssen J, Schoo HFM, Veenstra SC, Grogger W, Kothleitner G, Hofer F. Morphology determination of functional poly[2-methoxy-5-(3,7-dimethyloctyloxy)-1,4-phenylenevinylene]/poly[oxa-1,4-phenylene-1,2-(1-cyanovinylene)-2-methoxy,5-(3,7-dimethyloctyloxy)-1,4-phenylene-1,2-(2-cyanovinylene)-1,4-phenylene] blends as used for all-polymer solar cells. *Journal of Applied Polymer Science* 2005; **97**: 1001–1007.
50. Blache IA, Ramsdale CM, Thomas DS, Arias A-C, MacKenzie JD, Friend RH, Greenham NC, Donanld AM. Characterization of thin polymer blend films using ESEM - no charging, no staining. *Materials Research Society on Symposium and Proceedings* 2002; **707**: 41–47.
51. McNeill CR, Watts B, Thomsen L, Belcher WJ, Greenham NC, Dastoor PC. Nanoscale quantitative chemical mapping of conjugated polymer blends. *Nano Letters* 2006; **6**: 1202–1206.
52. McNeill CR, Watts B, Thomsen L, Ade H, Greenham NC, Dastoor PC. X-ray microscopy of photovoltaic polyfluorene blends: relating nanomorphology to device performance. *Macromolecules* 2007; **40**: 3263–3270.
53. Heriot SY, Jones RAL. An interfacial instability in a transient wetting layer leads to lateral phase separation in thin spin-cast polymer-blend films. *Nature Materials* 2005; **4**: 782–786.
54. Mihailetchi VD, Koster LJA, Blom PWM, Melzer C, de Boer B, van Duren JKJ, Janssen RAJ. Compositional dependence of the performance of poly(p-phenylene vinylene): methanofullerene bulk-heterojunction solar cells. *Advanced Functional Materials* 2005; **15**: 795–801.
55. Bates FS, Fredrickson GH. Block copolymers-designer soft materials. *Physics Today* 1999; **52**: 32–38.
56. Hilberer A, Moroni M, Gill RE, Brouwer HJ, Krasnikov VV, Pham TA, Malliaras GG, Veenstra SC, Werts MPL, van Hutten PF, Hadziioannou G. Photonic materials for electroluminescent, laser, and photovoltaic devices. *Macromolecular Symposia* 1997; **125**: 99–109.
57. Stalmach U, de Boer B, Videlot C, van Hutten PF, Hadziioannou G. Semiconducting diblock copolymers synthesized by means of controlled radical polymerization techniques. *Journal of American Chemical Society* 2000; **122**: 5464–5472.
58. Sun S, Fan Z, Wang Y, Haliburton J. Organic solar cell optimizations. *Journal of Material Science* 2005; **40**: 1429–1443.
59. Lindner SM, Huettner S, Chiche A, Thelakkat M, Krausch G. Charge separation at self-assembled nanostructured bulk interface in block copolymers. *Angewante Chemie International Edition* 2006; **45**: 3364–3368.
60. Sommer M, Lindner SM, Thelakkat M. Microphase-separated donor-acceptor diblock copolymers: influence of HOMO energy levels and morphology on polymer solar cells. *Advanced Functional Materials* 2007; **17**: 1493–1500.
61. Kietzke T, Neher D, Landfester K, Montenegro R, Guentner R, Scherf U. Novel approaches to polymer blends based on polymer nanoparticles. *Nature Materials* 2003; **2**: 408–412.
62. The effect of a thermal treatment is also applied in polymer: fullerene blends, see for example: Padinger F, Rittberger RS, Sariciftci NS. Effects of postproduction treatment on plastic solar cells. *Advanced Functional Materials* 2003; **13**: 84–88.

DOI: 10.1002/pip